A meshless method with enriched weight functions for fatigue crack growth

Marc Duflot*†, Hung Nguyen-Dang

Abstract

The meshless method is particularly appropriate to solve crack propagation problems. In this paper, the fatigue growth of cracks in two-dimensional bodies is considered. The analysis is based upon Paris' equation. New enriched weight functions are introduced in the meshless method formulation to capture the singularity at the crack tip. Simple problems show the accuracy and efficiency of this method. Then, it is applied to fatigue analysis of single- and multi-cracked bodies under mixed-mode conditions.

Key-words: meshless method, fracture mechanics, crack propagation, enriched weight functions

1 Introduction

The analysis of fatigue crack growth is essential to ensure the reliability of structures under cyclic loading conditions. Cracks, as a result of manufacturing defects or localized damage, may extend until brittle fracture occurs. In linear elastic fracture mechanics, cracks initiation is not considered. The propagation is modeled by successive crack extensions, which are determined by the stress intensity factors (SIFs) obtained after a stress analysis. The classic finite element method (FEM) is not appropriate to perform these successive analyses because the computational cost to remesh the body after each crack extension is prohibitive. To overcome this difficulty, there are mainly three different ways. Firstly, the *extended finite element method* [1] introduces local enrichment functions in the FEM approximation in order to represent the discontinuity of the displacement across the crack lines; enrichments are added as the cracks propagate through the elements. Secondly, the *boundary element method* [2, 3] permits to simulate the propagation simply by adding new boundary elements along cracks extensions. Thirdly, the *meshless method* [4, 5, 6, 7, 8, 9, 10, 11, 12, 13, 14] lets the cracks propagate among a set of nodes. The latter method is used in

*FNRS Research Fellow.

†Correspondence to: Marc Duflot, Fracture mechanics department, University of Liège, Chemin des chevreuils 1, 4000 Liège, Belgium. E-mail: m.duflot@ulg.ac.be.

this paper and is improved by taking into account the near-tip displacement field to accurately compute the life of structures.

An outline of the paper is as follows. In Section 2, we briefly present the basis of the meshless method and some issues related to its use in fracture mechanics. Then in Section 3, we concentrate upon the way to accurately represent the near-tip displacement field with this method. We recall that a nodal refinement near the tip is the way to capture the singularity used in most papers, and that an enriched basis functions set or an enriched trial functions set can also be used. Finally, we describe our new method: it consists in adding three nodes with special weight functions at each crack tip. In Section 4, we explain the steps of a fatigue crack growth analysis: the computation of stress intensity factors, the prediction of the propagation direction and of the increment length at each crack tip if the cracks are stable, the instability criterion, and the determination of the number of cycles until unstable crack growth. We give several numerical in Section 5 and draw the conclusions in Section 6.

2 Meshless method

We use the numerical method to solve partial differential equations (PDEs) without the need to build a mesh that was introduced in Reference [15] under the name *diffuse finite element method* and in Reference [16] under the name *element-free Galerkin method*. In this paper, we choose to use the name *meshless method* commonly used nowadays. The fundamental principle consists in approximating the unknown field of the PDEs by a *moving least-squares approximation* (MLSA). This approximation is briefly recalled hereafter. We refer to both previously cited papers for the details.

Consider a set of N nodes scattered in a domain Ω and let $\mathbf{x}_i$ be the coordinates of node i. The MLSA $\mathbf{u}^h(\mathbf{x})$ of a (multi-dimensional) field $\mathbf{u}(\mathbf{x})$ in Ω is:

$$\mathbf{u}^h(\mathbf{x}) = \sum_{i=1}^{N} \phi_i(\mathbf{x})\,\mathbf{u}_i \tag{1}$$

where $\mathbf{u}_i$ is the value of the field $\mathbf{u}$ at $\mathbf{x}_i$ and ϕ_i is the shape function of node i, given by

$$\phi_i(\mathbf{x}) = \mathbf{c}^{\mathrm{T}}(\mathbf{x})\,\mathbf{p}(\mathbf{x}_i)\,w_i(\mathbf{x}) \tag{2}$$

where $\mathbf{p}(\mathbf{x})$ is a set of basis functions, $w_i(\mathbf{x})$ is a weight function associated with node i and

$$\mathbf{c}(\mathbf{x}) = \mathbf{A}^{-1}(\mathbf{x})\,\mathbf{p}(\mathbf{x}) \tag{3}$$

with

$$\mathbf{A}(\mathbf{x}) = \sum_{i=1}^{N} w_i(\mathbf{x})\,\mathbf{p}(\mathbf{x}_i)\,\mathbf{p}^{\mathrm{T}}(\mathbf{x}_i) \tag{4}$$

In practice, the weight functions are positive so that the $\mathbf{A}$ matrix is definite positive and that the approximation is well-behaved. Moreover, a small domain Ω_i containing $\mathbf{x}_i$ is associated with node i such that $w_i(\mathbf{x})$, and as a result $\phi_i(\mathbf{x})$,

equal zero outside Ω_i. This choice is made in order to give the approximation a local character and to restrict the sums in Equations (1) and (4) to a few terms. Finally, the common choice in the literature is that $w_i(\mathbf{x})$ decreases with the distance between $\mathbf{x}_i$ and $\mathbf{x}$, in such a way that the nearer a node is to a point, the greater it influences this point; but, this choice is revised in Section 3.

The meshless method for the resolution PDEs of consists in using the shape functions (2) as the test functions and the trial functions in the variational principle of these PDEs. In this paper, the PDEs under consideration are the equilibrium equations of two-dimensional, homogeneous, isotropic and linear-elastic solids undergoing small displacements. We refer to the overview paper [9] for the issues related to the enforcement of the essential boundary conditions and to the numerical integration, and for the resulting stiffness matrix and load vector.

2.1 Choice of the basis and of the weights

In the following, we always use a linear basis: $\mathbf{p}^{\mathrm{T}} = [1, x, y]$, which proved to be a good trade-off between speed and efficiency. But, the enriched method described later also works with another basis. We decide to use the same weight for each regular node (in contrast with the enriched nodes described later): a quartic weight function on a circular support

$$w_i(\mathbf{x}) = S_4(s) \tag{5}$$

where we use the quartic spline

$$S_4(s) = \begin{cases} 1 - 6s^2 + 8s^3 - 3s^4 & \text{if } s \leq 1 \\ 0 & \text{if } s > 1 \end{cases} \tag{6}$$

and the normalized distance is

$$s = \frac{\|\mathbf{x} - \mathbf{x}_i\|}{R_i} \tag{7}$$

with R_i the radius of the influence domain of node i. These radii must be large enough so that each point of the domain is covered by at least 3 supports (3 being the size of the basis). According to our experience, $R_i = 1.7 \times h$, where h is the characteristic nodal spacing distance, is a good choice.

It is useful for the explanation of the enriched method to plot a weight function and a shape function. So, consider 5×5 nodes regularly distributed in a domain $[-2, 2] \times [-2, 2]$ ($h = 1$). The weight function and the shape function of the central node located at $(0, 0)$ are plotted in Figure 1. We see that these functions exhibit the same shape although their amplitude is different. More plots showing the resemblance between the weight functions and the shape functions can be found in Reference [17].

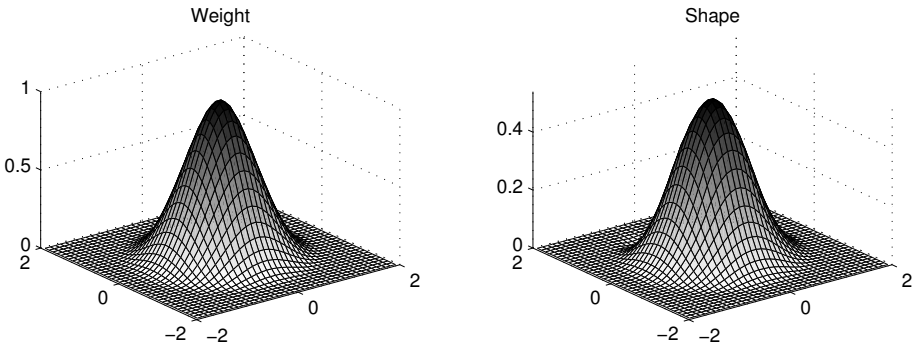

Figure 1: The resemblance between a weight function and a shape function

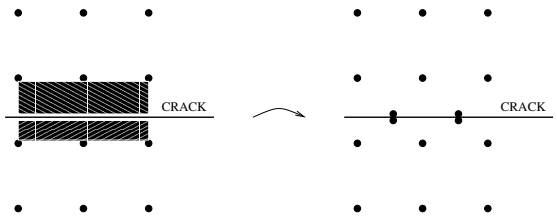

Figure 2: Additional nodes at both sides of the crack

2.2 Modified weights in presence of cracks

The distance s in Equation (5) must be modified if the line segment joining $\mathbf{x}_i$ and $\mathbf{x}$ crosses a crack line in order to represent the displacement discontinuity across this line. As in Reference [18], s becomes the total length of the shortest path from $\mathbf{x}_i$ to $\mathbf{x}$ that lies entirely within the domain (divided by the radius of the support):

$$s = \frac{\|\mathbf{x} - \mathbf{x}_c\| + \|\mathbf{x}_c - \mathbf{x}_i\|}{R_i} \tag{8}$$

where $\mathbf{x}_c$ are the coordinates of the crack tip near $\mathbf{x}_i$.

2.3 Additional nodes in presence of cracks

If a node is located on a crack, it is split in two; one node is moved of a small distance at one side of the crack and the other is moved of the same amount at the other side. Moreover, it is good to add some nodes at each side of the crack as illustrated in Figure 2. In this way, the shaded areas where the MLS approximation is an extrapolation disappear. In our experience, this always improves the quality of the solution.

3 Near-tip field enrichment

As explained in the introduction, the meshless method is particularly suitable to simulate crack propagation. But, special care must be taken in order to precisely model the high gradient of the displacement near the crack tip. Otherwise, the SIFs are underestimated and the life of the structures overestimated. Let us recall that, in the absence of mode III, the near-tip displacement field is given by:

$$\mathbf{u}(\mathbf{x}) = K_I \mathbf{Q}_I(\mathbf{x}) + K_{II} \mathbf{Q}_{II}(\mathbf{x}) \tag{9}$$

$$\mathbf{Q}_I(\mathbf{x}) = \frac{1}{2\mu}\sqrt{\frac{r}{2\pi}} \begin{pmatrix} \cos\left(\frac{\theta}{2}\right)\left[\kappa - 1 + 2\sin^2\left(\frac{\theta}{2}\right)\right] \\ \sin\left(\frac{\theta}{2}\right)\left[\kappa + 1 - 2\cos^2\left(\frac{\theta}{2}\right)\right] \end{pmatrix} \tag{10}$$

$$\mathbf{Q}_{II}(\mathbf{x}) = \frac{1}{2\mu}\sqrt{\frac{r}{2\pi}} \begin{pmatrix} \sin\left(\frac{\theta}{2}\right)\left[\kappa + 1 + 2\cos^2\left(\frac{\theta}{2}\right)\right] \\ \cos\left(\frac{\theta}{2}\right)\left[-\kappa + 1 + 2\sin^2\left(\frac{\theta}{2}\right)\right] \end{pmatrix} \tag{11}$$

where K_I and K_{II} are mode I and mode II SIFs respectively, r is the distance to the tip, θ is the angle measured from a line ahead of the crack ($\theta \in [-\pi, \pi]$), μ is the shear modulus and κ is the Kolosov constant. We first review the existing methods to address this difficulty and then explain our method

3.1 Review of existing methods

To address the problem of this high gradient, in References [4, 5, 6], the spatial discretization is refined near the tip. These nodal arrangements are moved with the crack tip at each step of the quasi-static propagation. For dynamic crack propagation, an Arbitrary Lagrangian-Eulerian formulation is used in Reference [12] to continuously relocate the nodes. In References [7, 8, 13], the spatial discretization is fine in the whole domain; this leads of course to high computation costs. Another approach to this problem of the singularity is to use an enriched basis: either a fully enriched basis

$$\mathbf{p}^{\mathrm{T}} = \left[1, x, y, \sqrt{r}\cos\left(\frac{\theta}{2}\right), \sqrt{r}\sin\left(\frac{\theta}{2}\right), \sqrt{r}\sin\left(\frac{\theta}{2}\right)\sin(\theta), \sqrt{r}\cos\left(\frac{\theta}{2}\right)\sin(\theta)\right]$$

as in References [11, 14] or a partially enriched basis $\mathbf{p}^{\mathrm{T}} = [1, x, y, \sqrt{r}]$ as in Reference [14]. These methods work well, particularly the fully enriched basis, but this fully enriched method is quite computationally expensive because a 7×7 matrix must be inverted at each Gauss point, see Equations (3) and (4), instead of a 3×3 matrix as it is the case with the linear basis. To reduce this cost, it is possible to use the enriched method in a region surrounding the crack tip and the classic method away from the crack tip with a transition region in between. Finally, the enrichment of the trial functions is also proposed in Reference [11]:

$$\mathbf{u}^h(\mathbf{x}) = \sum_{i=1}^{N} \phi_i(\mathbf{x})\,\mathbf{u}_i + \sum_{j=1}^{n_c} \left[\mathbf{Q}_I^j(\mathbf{x})\,k_I^j + \mathbf{Q}_{II}^j(\mathbf{x})\,k_{II}^j\right] \tag{12}$$

where n_c is the number of crack tips and k_I^j and k_{II}^j are additional degrees of freedom associated with mode I and mode II respectively at tip j. It is quite heavy to introduce this trial function into the variational principle, but the method works well. This comes at the cost of an increase in the band-width of the stiffness matrix because the additional degrees of freedom interact with every other degrees of freedom. Again, it is possible to restrict the enrichments in regions surrounding the crack tips to reduce this cost.

3.2 Enrichment with special weight functions

Our enriched method consists in adding some nodes with special weight functions at each tip. Using the Equations (2) to (4) of the MLSA, each node and its associated weight function give a shape function that enrich the set of regular shape functions. Our aim is that these shape functions behave in a way similar to the near tip displacement field given in Equations (9) to (11). To that end, we choose the *weight functions* to behave in a way similar to Equations (10) and (11) and we expect that the resulting *shape functions* resemble them — as it is the case for the regular nodes in Figure (1).

More precisely, the following criteria guide us in the choice of the special weight functions:

1. The weight functions should vary as $\sqrt{r}$ for small r: this is the main criterion in order to obtain by derivation a stress field that varies as $\frac{1}{\sqrt{r}}$ for small r.
2. They should be positive: this is requested for the positive definiteness of the $\mathbf{A}$ matrix, given by Equation (4).
3. They should have an angular variation of the same kind as those in Equations (10) and (11): this suggests using $\cos\left(\frac{\theta}{2}\right)$ and $\sin\left(\frac{\theta}{2}\right)$.
4. They should be zero outside a circular support like the regular weights: this provides the enrichment with a local character.

According to some experiments, the use in conjunction of the three following weights appears to be a good choice:

$$w_c(\mathbf{x}) = \alpha\sqrt{r}\cos\left(\frac{\theta}{2}\right) S_4(s) \tag{13}$$

$$w_p(\mathbf{x}) = \alpha\sqrt{r}\left[1+\sin\left(\frac{\theta}{2}\right)\right] S_4(s) \tag{14}$$

$$w_m(\mathbf{x}) = \alpha\sqrt{r}\left[1-\sin\left(\frac{\theta}{2}\right)\right] S_4(s) \tag{15}$$

In these equations,

- The indices c, p and m respectively stand for "cos", "plus sin" and "minus sin".

- S_4 is the quartic spline function of Equation (6) and the normalized distance s is again given by Equation (7), with the coordinates of the three nodes being identical: $\mathbf{x}_c = \mathbf{x}_p = \mathbf{x}_m = \mathbf{x}_{tip}$.
- We also choose an identical radius of the influence domain, which normalizes the distance in Equation (7): $R_c = R_p = R_m$. We choose that this radius is equal to the minimum of the radius of the neighboring regular nodes and the distance between the tip and the first crack tip. So, the domain of influence does not contain any kink.
- The α factor controls the amplitude of the enriched weight compared with the amplitude of the regular nodes; $\alpha = 1$ is a reasonable choice.

We observe that the three functions meet the previous criteria:

1. At $r = 0$, $s = 0$ and the derivative of the spline function equals zero: $S_4'(s) = 0$. So, for θ fixed, the partial derivatives of the special weight functions $\frac{\partial w_{c,p,m}}{\partial r}$ are proportional to $\frac{1}{\sqrt{r}}$ at the tip. These derivatives appear in the derivatives of the shape function by derivation of Equation (2), which in turn provide the desired singularity to the stress field.
2. They are positive since the quartic spline is positive and so are $\cos\left(\frac{\theta}{2}\right)$, $1 + \sin\left(\frac{\theta}{2}\right)$ and $1 - \sin\left(\frac{\theta}{2}\right)$ $(\theta \in [-\pi, \pi])$.
3. The three special weight functions are dominant in three different areas around the tip. w_c is dominant in front of the crack, w_p is dominant on the side of the crack where $\theta = \pi$ and w_m is dominant on the other side where $\theta = -\pi$. Moreover, w_p and w_m are discontinuous along the crack.
4. The presence of the spline provides the local character of the special functions.

In Figure 3, we illustrate the shape functions ϕ_c, ϕ_p and ϕ_m that result from the chosen special weight functions. We use the same set of 5×5 nodes as in Figure 1 and a crack whose tip is located at $(0, 0)$. The three enriched nodes are added at the tip. The radius of their support is the same as those of the regular nodes. We plot the enriched shape functions ϕ_c, ϕ_p and ϕ_m and also show the plane with the nodes and the crack under the same perspective. We observe that they have the desired properties:

1. They vary as $\sqrt{r}$ near the tip and like a spline further.
2. They are dominant in different areas around the tip.
3. ϕ_p and ϕ_m exhibit a discontinuity along the crack that strengthens the displacement discontinuity provided by the modification of the weights explained in Section 2.2. This will permit to represent more accurately the opening of the crack.

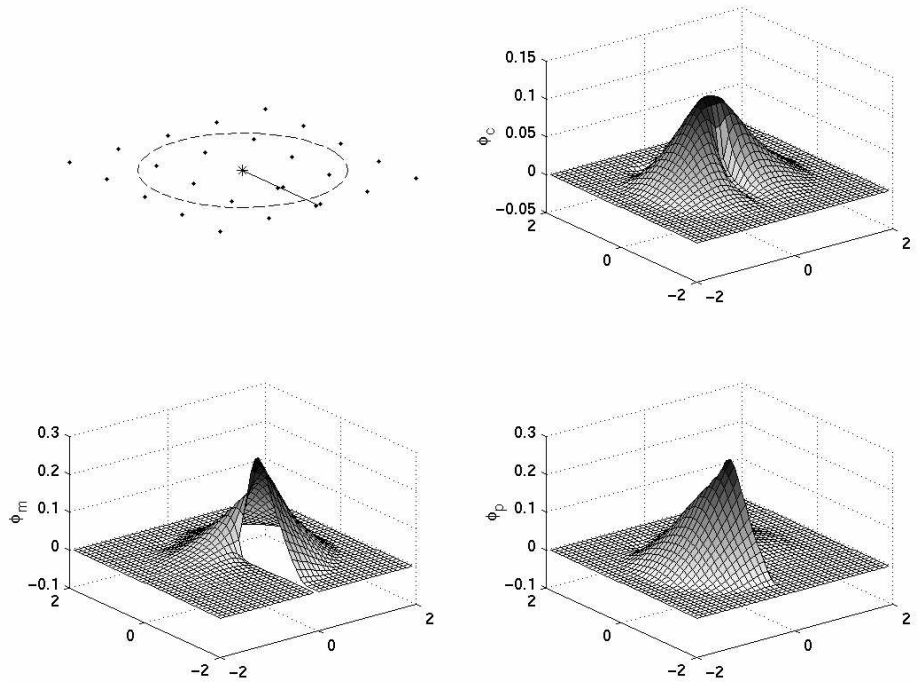

Figure 3: Enriched shape functions

We emphasize on the fact that the enriched functions are introduced easily and inexpensively in a meshless method formulation. Indeed, there is no need to manage an enriched area, a normal area and a transition area like with the other enriched methods described at the beginning of this section.

4 Fatigue crack growth analysis

The stress intensity factors are calculated by conservation integrals converted into a domain form [19]. In mixed-mode problems, auxiliary solutions (10) and (11) are used in two interaction conservation integrals to directly obtain both factors, see Reference [20]. The integration domain is a square centered on the tip and the half-side of this square is equal to the length of a crack increment. The domain thus does not contain any kink. For constant amplitude cyclic loadings, the range of the SIF is defined as

$$\Delta K = K_{max} - K_{min} \tag{16}$$

where K_{max} and K_{min} are the SIFs corresponding to the maximum (σ_{max}) and minimum (σ_{min}) applied loads respectively.

In general, the crack path is a curved path. In our analysis, crack propagation is simulated by successive linear increments. We have to determine the

direction and the length of these increments. Several criteria exist for the determination of the direction of crack growth under mixed-mode loading. The most important are: maximum principal stress criterion, maximum energy release rate criterion and minimum strain energy density criterion. These criteria predict kink angles of almost the same size, especially in the case of small or medium mixed-mode ratio $\frac{K_{II}}{K_I}$. In the present work, the maximum principal stress criterion is used, which postulates that the crack growth occurs in a direction perpendicular to the maximum principal stress. Thus, at each crack tip, the local direction of crack growth θ_c is determined by the condition that the local shear stress is zero, that is (see for example Reference [21] for details):

$$K_I \sin\theta_c + K_{II}\left(3\cos\theta_c - 1\right) = 0 \tag{17}$$

Solving this equation gives

$$\theta_c = 2\arctan\left(\frac{K_I - \sqrt{K_I^2 + 8K_{II}^2}}{4K_{II}}\right) \tag{18}$$

According to this criterion, the equivalent mode I SIF is

$$K_{Ieq} = K_I \cos^3\frac{\theta_c}{2} - 3K_{II}\cos^2\frac{\theta_c}{2}\sin\frac{\theta_c}{2} \tag{19}$$

This equivalent stress intensity factor is useful in the unstable fracture criterion below and in the following propagation law. To model the stable crack propagation, we use the generalized Paris' law:

$$\frac{\mathrm{d}a}{\mathrm{d}N} = C\left(\Delta K_{Ieq}\right)^m \tag{20}$$

where C and m are material properties, a is the crack length, N is the number of loading cycles and ΔK_{Ieq} is obtained by Equation (19) with ΔK_I and ΔK_{II} instead of K_I and K_{II}. The number of loading cycles required to extend the crack from the initial length to a given length is evaluated by integrating this law with a trapezoidal rule.

A compromise must be made regarding the value of the linear increment length Δa. If it is too small, the influence domain of the enriched nodes and the integration domain of the conservation integral are small and this leads to inaccurate results. If it is too long, the piecewise linear path can not precisely represent the real curved path. For single-cracked bodies, Δa is kept constant. For multi-cracked bodies, we choose a constant value for the maximum increment length Δa_{max}, and after each step we select the principal crack tip as the tip where ΔK_{Ieq} is maximum and then at every crack tip the increment is given by

$$\Delta a = \Delta a_{max}\left(\frac{\Delta K_{Ieq}}{\Delta K_{Ieq,max}}\right)^m \tag{21}$$

where $\Delta K_{Ieq,max}$ is the range of the equivalent mode I SIF at the principal crack tip and m is the exponent in Paris' law. Accordingly, the increment at

Half-length of the crack a	0.1	0.2	0.3	0.4	0.5	0.6	0.7
F_I — Reference [22]	1.014	1.055	1.123	1.216	1.334	1.481	1.68
F_I — without enrichment	0.967	1.010	1.075	1.162	1.272	1.408	1.586
Error — without enrichment	4.6%	4.3%	4.3%	4.4%	4.6%	4.9%	5.6%
F_I — with enrichment	1.004	1.057	1.125	1.217	1.333	1.477	1.668
Error — with enrichment	0.99%	0.15%	0.14%	0.05%	0.09%	0.26%	0.74%

Table 1: Mode I normalized stress intensity factors for the centered crack problem

the principal crack tip is equal to Δa_{max} and is smaller than this value at other crack tips. We note that the principal tip can change during the propagation.

Instability of the cracked body occurs when $K_{Ieq,max,max} > K_{Ic}$ where K_{Ic} is a material property called the fracture toughness. $K_{Ieq,max,max}$ is the equivalent mode I SIF corresponding to σ_{max} at the principal crack tip. This condition is the stopping criterion in our method: crack increments are added until this condition is met.

5 Numerical results

5.1 Single centered crack

The first example is a single crack, centered in a square plate under uniform tension. The square side is 2 units and the crack length $2a$ varies from 0.2 to 1.4 units. A set of 21×21 uniformly spaced nodes is used. A number of nodes, which grows with the crack, are located on the crack so they are splitted in two. We solve the problem with the three enriched nodes at both tips on one hand and without them on the other hand in order to compare the results. The radius of the support of each (regular or enriched) node is 0.17 units. The integration is performed by dividing the square in 20×20 cells, with 8×8 Gauss points in each cell. The fatigue crack growth theory is not applied for this problem; the crack grows by step of 0.1 units at each tip. This is justified because the SIFs are the same at both tips.

In Table 1, we compare the values of $F_I = \frac{K_I}{\sigma\sqrt{\pi a}}$ for this range of a without and with the 3 enrichments, with the solution in Reference [22]. This table shows the significant improvement of the results when the enriched method is used. For $a = 0.1$, the computed SIF is not as good as for $a \geq 0.2$; this is probably due to the overlapping of the supports of the 2 enrichments. The computational overhead of the enriched method is weak — only 4% of the CPU cost of the classic method.

Length of the crack a	0.2	0.4	0.6	0.8	1.0	1.2	1.4	1.6
F_I — Reference [22]	1.23	1.49	1.85	2.32	3.01	4.15	6.40	12.0
F_I — without enrichment	1.151	1.404	1.745	2.190	2.823	3.856	5.843	10.55
Error — without enrichment	6.4%	5.8%	5.7%	5.6%	6.2%	7.1%	8.7%	12.1%
F_I — with enrichment	1.217	1.477	1.836	2.306	2.978	4.086	6.239	11.45
Error — with enrichment	1.0%	0.86%	0.78%	0.62%	1.1%	1.6%	2.5%	4.6%

Table 2: Mode I normalized stress intensity factors for the edge crack problem

5.2 Single edge crack

In Table 2, we present the results for a single edge crack in a square plate under uniform tension. We use the same geometry and the same set of nodes as in the previous section. We see that the enriched method gives once again far better results than the classic method.

5.3 Single centered angled crack

To validate the new method for mixed-mode problems, we consider a static angled crack (18 units long) in a rectangular plate (90×180) under uniform tension ($\sigma = 160$). A set of 19×37 uniformly spaced nodes is used and 4 nodes are added on each side of the crack (Figure 4) to avoid the problem described in Section 2.3 with the "shaded" area of Figure 2. The radius of the support of each (regular or enriched) node is 8.5 units. The integration is performed on 18×36 cells, with 8×8 Gauss points in each cell. Some cells are cut by the crack but the number of integration points in each cell appears to be sufficient and there is no need to divide these cells or to add Gauss points in them.

We plot in Figure 5 mode I and mode II stress intensity factors for some values of the crack angle obtained with or without the enrichment. The enrichment improves the results for every value of the angle and shows very good agreement with Reference [22].

5.4 Single edge angled crack

The fatigue growth of an edge angled crack that we study in this section is a more challenging problem than those studied before. We use the same dimensions, the same material properties and the same loading as in Reference [3] to perform a comparison. A rectangular plate ($100mm \times 200mm$) with a crack ($a_0 = 20mm$) that makes an angle 40° with a line perpendicular to the edge is submitted to a cyclic tension ($\sigma_{max} = 40\ N/mm$, $\sigma_{min} = 0$) at both ends. The material

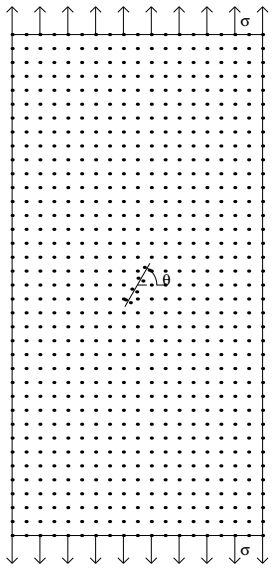

Figure 4: Set of nodes for the plate with an angled crack

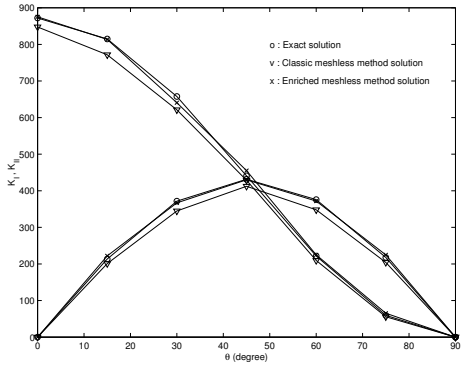

Figure 5: Stress intensity factors for the centered angled crack problem

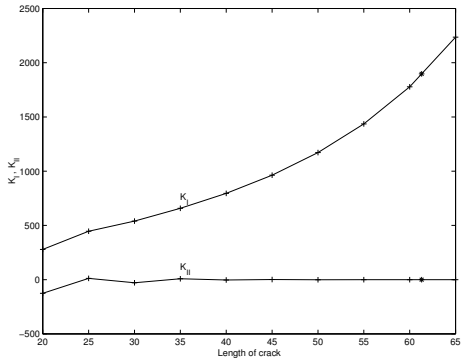

Figure 6: Stress intensity factors for the edge angled crack problem

properties are as follows:

$E = 74000\, N/mm^2$	elastic modulus	
$\nu = 0.3$	Poisson ratio	
$K_{Ic} = 1897.36\, N/mm^{\frac{3}{2}}$	fracture toughness	(22)
$m = 3.32$	Paris exponent	
$C = 2.087136 \times 10^{-13}$	Paris constant	

We use a regular set of 21×41 nodes plus 5 nodes on each side of the initial crack. There is a node at the intersection between the crack and the edge that is splitted in two. The 3 enriched nodes at the crack tip are used. When the crack grows, these enriched nodes move with the crack tip and we add 1 regular node on each side of the crack increment. The radius of the support of the enriched nodes is equal to $8.5\, mm$. The crack increment length Δa and the radius of the support of the enriched nodes are equal to $5\, mm$. The integration is performed on 20×40 cells, with again 8×8 Gauss points in each cell.

The variation of the SIFs with the crack length and the fatigue-life diagram are presented in Figures 6 and 7 respectively. On these figures, the asterisk represents the failure. The total crack length is $61.3\, mm$ when unstable crack growth occurs and the life of the structure is evaluated as 131411 cycles. This is in good agreement with results in Reference [3]: $61.2\, mm$ for the final length and 144885 cycles. The crack path is plotted in Figure 8. We observe a sudden change of the direction of the crack at the beginning of the propagation. This change is such that mode II SIF vanishes. After that initial kink, the crack grows in a straight line.

5.5 Two internal non-colinear cracks

A rectangular plate ($90mm \times 180mm$) with 2 internal, parallel, non-colinear and non-angled cracks (length = $10\, mm$ for both) is submitted to a cyclic tension ($\sigma_{max} = 160\, N/mm$, $\sigma_{min} = 0$) at both ends. The horizontal distance between the two tips close to each other is $15\, mm$ and the vertical distance is $5\, mm$. The

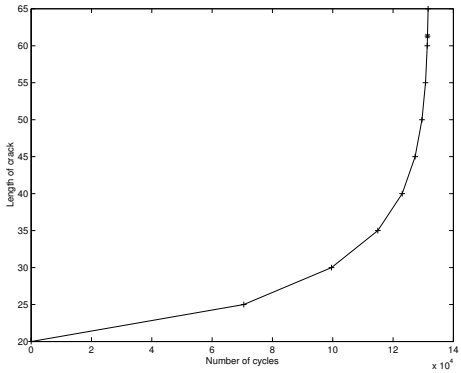

Figure 7: Fatigue-life diagram for the edge angled crack problem

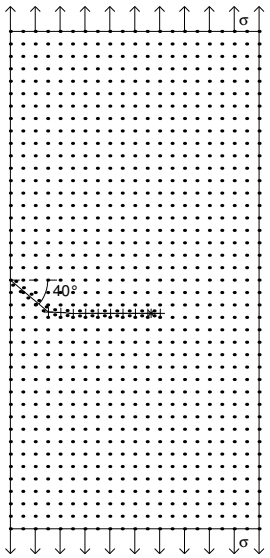

Figure 8: Crack path for the edge angled crack problem

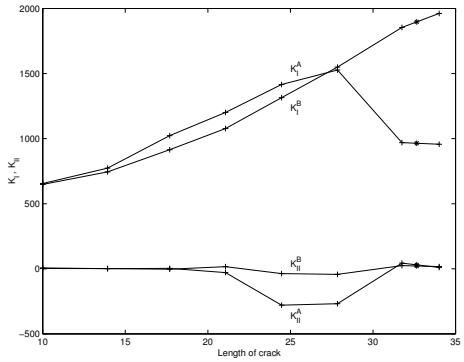

Figure 9: Stress intensity factors for the "two internal cracks" problem

material properties are the same as in the previous section. We use a regular set of 19×37 nodes plus 2 nodes on each side of both initial cracks (radius=$8.5\,mm$) and the 3 enriched nodes at each crack tip. When the crack grows, the enriched nodes move and regular nodes are added as in Section 5.4. The maximum crack increment length Δa_{max} is equal to $2\,mm$. The radius of the support of the enriched nodes at each tip is equal to the increment of the crack of the previous step at this tip. The integration is performed on 18×36 cells, with again 8×8 Gauss points in each cell.

The evolution of the SIFs at the most interior crack tip (A) and at the crack tip near the edge (B) with the crack length is plotted in Figure 9. The fatigue-life diagram and the crack paths are presented in Figures 10 and 11 respectively. In the beginning, it is a pure mode I state and the SIFs at A and B are about the same. Then, mode I factor at A increases quicker than at B and mode II factor at A becomes negative so that the crack paths curve towards the other crack. But, when the crack tips A overlap, the stress intensity factors tend to decrease, while mode I factor increases continuously at B. Finally, the equivalent mode I SIF at B exceeds the fracture toughness and unstable fracture occurs at the crack tips B. This prediction of the fatigue crack growth path is in good agreement with the experimental results reported in Reference [23]. The life of the structure is evaluated as 6792 cycles, which is in good agreement with Reference [3].

6 Conclusions

Enriched weight functions were introduced in a meshless method formulation to capture the singularity of the stress field at crack tips. They permitted to accurately evaluate the stress intensity factors with few degrees of freedom. The method was applied to the simulation of fatigue fracture of single- or multi-cracked bodies under constant amplitude cyclic loading with the help of Paris' law. The real curved path of crack growth was simulated by piece-wise linear

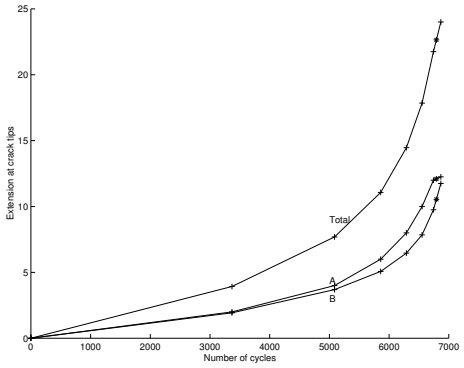

Figure 10: Fatigue-life diagram for the "two internal cracks" problem

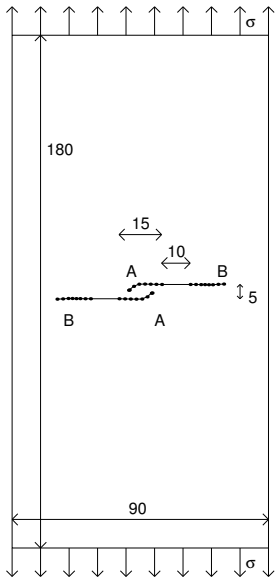

Figure 11: Crack path for the "two internal cracks" problem

increments. The direction of crack growth was predicted by the maximum principal stress criterion. Numerical results showed good agreement with boundary element method results.

Finally, we find it of interest to quantify the efficiency of the meshless method. To the best of our knowledge, it is the first time this is done. The complete resolution of the problem in Section 5.5, which was solved in 8 steps (each step comprising from 719 to 783 nodes, over $40,000$ Gauss points and a linear system solving), only took 23 seconds on a 2.8 GHz personal computer with our optimized code. This proves that the meshless method is really suitable to solve crack propagation problems.

Acknowledgements

The support of the Belgian National Fund for Scientific Research (F.N.R.S.) to Marc Duflot is gratefully acknowledged.

References

[1] Moës N, Dolbow J, Belytschko T. A finite element method for crack growth without remeshing. *International Journal for Numerical Methods in Engineering* 1999, **46**:131–150.

[2] Portela A, Aliabadi M, Rooke D. The dual boundary element method: Effective implementation for crack problem. *International Journal for Numerical Methods in Engineering* 1991, **33**:1269–1287.

[3] Yan AM, Nguyen-Dang H. Multiple-cracked fatigue crack growth by BEM. *Computational Mechanics* 1995, **16**:273–280.

[4] Belytschko T, Gu L, Lu YY. Fracture and crack growth by element-free Galerkin methods. *Modelling Simulation for Materials Science and Engineering* 1994, **2**:519–534.

[5] Belytschko T, Lu YY, Gu L. Crack propagation by element-free Galerkin methods. *Engineering Fracture Mechanics* 1995, **51**(2):295–315.

[6] Belytschko T, Lu YY, Gu L, Tabbara M. Element-free Galerkin methods for static and dynamic fracture. *International Journal of Solids and Structures* 1995, **32**(17–18):2547–2570.

[7] Lu YY, Belytschko T, Tabbara M. Element-free Galerkin method for wave propagation and dynamic fracture. *Computer Methods in Applied Mechanics and Engineering* 1995, **126**:131–153.

[8] Belytschko T, Tabbara M. Dynamic fracture using element-free Galerkin methods. *International Journal for Numerical Methods in Engineering* 1996, **39**:923–938.

[9] Belytschko T, Krongauz Y, Organ D, Fleming M, Krysl P. Meshless methods: An overview and recent developments. *Computer Methods in Applied Mechanics and Engineering* 1996, **139**:3–47.

[10] Organ D, Fleming M, Terry T, Belytschko T. Continuous meshless approximations for nonconvex bodies by diffraction and transparency. *Computational Mechanics* 1996, **18**:1–11.

[11] Fleming M, Chu YA, Moran B, Belytschko T. Enriched element-free Galerkin methods for crack tip fields. *International Journal for Numerical Methods in Engineering* 1997, **40**:1483–1504.

[12] Ponthot JP, Belytschko T. Arbitrary lagrangian-eulerian formulation for element-free Galerkin method. *Computer Methods in Applied Mechanics and Engineering* 1998, **152**:19–46.

[13] Tabbara MR, Stone CM. A computational method for quasi-static fracture. *Computational Mechanics* 1998, **22**:203–210.

[14] Rao BN, Rahman S. An efficient meshless method for fracture analysis of cracks. *Computational Mechanics* 2000, **26**:398–408.

[15] Nayroles B, Touzot G, Villon P. Generalizing the finite element method: Diffuse approximation and diffuse elements. *Computational Mechanics* 1992, **10**:307–318.

[16] Belytschko T, Lu YY, Gu L. Element-free Galerkin methods. *International Journal for Numerical Methods in Engineering* 1994, **37**:229–256.

[17] Atluri SN, Kim HG, Cho JY. A critical assessment of the truly meshless local Petrov-Galerkin and local boundary integral equation methods. *Computational Mechanics* 1999, **24**:348–372.

[18] Belytschko T, Krongauz Y, Fleming M, Organ D, Liu WK. Smoothing and accelerated computations in the element-free Galerkin method. *Journal of Computational and Applied Mathematics* 1996, **74**:111–126.

[19] Moran B, Shih CF. Crack tip and associated domain integrals from momentum and energy balance. *Engineering Fracture Mechanics* 1987, **27**(6):615–641.

[20] Yau JF, Wang SS, Corten HT. A mixed-mode crack analysis of isotropic solids using conservation laws of elasticity. *Journal of Applied Mechanics* 1980, **47**:335–341.

[21] Broek D. *Elementary Engineering Fracture Mechanics*. Noordhoff International Publishing, Leyden, 1974.

[22] Murakami Y, editor. *Stress Intensity Factors Handbook*. Pergamon Press, 1987.

[23] Tu ST, Cai RY. A coupling of boundary elements and singular integral equation for the solution of the fatigue cracked body. *Stress Analysis*, pages 239–247, 1993.